NEUROSCIENCE
RESEARCH ARTICLE
K. P. Nguyen et al. / Neuroscience 466 (2021) 260–272

# Distinct Kinematic Adjustments over Multiple Timescales Accompany Locomotor Skill Development in Mice

**Katrina P. Nguyen,** [a,b] **Abhinav Sharma,** [a,b] **Mauricio Gil-Silva,** [d] **Aryn H. Gittis** [c,d1] **and Steven M. Chase** [a,c1*]

[a] *Department of Biomedical Engineering, Carnegie Mellon University, Pittsburgh, PA, United States*

[b] *Center for the Neural Basis of Computation, Carnegie Mellon University, Pittsburgh, PA, United States*

[c] *Neuroscience Institute, Carnegie Mellon University, Pittsburgh, PA, United States*

[d] *Department of Biological Sciences, Carnegie Mellon University, Pittsburgh, PA, United States*

**Abstract—Robust locomotion is critical to many species' survival, yet the mechanisms by which efficient locomotion is learned and maintained are poorly understood. In mice, a common paradigm for assaying locomotor learning is the rotarod task, in which mice learn to maintain balance atop of an accelerating rod. However, the standard metric for learning in this task is improvements in latency to fall, which gives little insight into the rich kinematic adjustments that accompany locomotor learning. In this study, we developed a rotarod-like task called the RotaWheel in which changes in paw kinematics are tracked using high-speed cameras as mice learn to stay atop an accelerating wheel. Using this device, we found that learning was accompanied by stereotyped progressions of paw kinematics that correlated with early, intermediate, and late stages of performance. Within the first day, mice sharpened their interlimb coordination using a timed pause in the forward swing of their forepaws. Over the next several days, mice reduced their stride length and took shorter, quicker steps. By the second week of training, mice began to use a more variable locomotor strategy, where consecutive overshoots or undershoots in strides were selected across paws to drive forward and backward exploration of the wheel. Collectively, our results suggest that mouse locomotor learning occurs through multiple mechanisms evolving over separate time courses and involving distinct corrective actions. These data provide insights into the kinematic strategies that accompany locomotor learning and establish an experimental platform for studying locomotor skill learning in mice.**


**Key words: motor learning, locomotion, skill acquisition.**

## INTRODUCTION

Locomotion is central to many species' survival, whether it be for avoiding predators, catching prey, finding mates, or foraging for food. Robust locomotion is achieved through the precise coordination of muscle activity across the entire body. When locomotion is disrupted, due to injury, growth, or changes in terrain, the activity of dozens of muscles acting across tens of degrees-of-freedom must adjust to recover rapid, stable movement. How is this learning accomplished?

In mice, a standard paradigm for assaying locomotor coordination is the rotarod task, in which animals are trained to balance on top of a slowly accelerating wheel (Jones and Roberts, 1968). This paradigm has been widely used to evaluate motor skill learning (Buitrago et al., 2004; Costa et al., 2004; Yin et al., 2009), motor dysfunction in disease models (Crawley, 1999; Sausbier et al., 2004; Monville et al., 2006; Campos et al., 2013; Carvalho et al., 2013), and the effects of experimental drugs on balance and motor coordination (Brooks et al., 2012; Durieux et al., 2012). To successfully complete the task, a mouse must continually adjust its running pattern to match the speed demands of the accelerating rod. However, the standard reported 'latency to fall' metric (i.e., the time the mouse can remain on the accelerating rod before falling off) does not capture the rich kinematic adjustments that underlie locomotor learning. A detailed understanding of these learning-related kinematic changes could provide insights into how different brain areas and plasticity mechanisms are engaged at various stages of the learning process.

To overcome this challenge, we developed a rotarod-like task called the RotaWheel to study the kinematic changes that accompany locomotor learning. In this task, mice learn to stay balanced on top of a gradually accelerating wheel while paw kinematics and body position are continuously monitored through side-

*Correspondence to: S. M. Chase, 115N Mellon Institute, Carnegie Mellon University, 4400 Fifth Ave., Pittsburgh, PA 15213, United States.
[1] These authors contributed equally

https://doi.org/10.1016/j.neuroscience.2021.05.002
0306-4522/

mounted high-speed cameras. Over a two-week period, we observed three distinct phases of kinematic adjustments. The first phase (early learning) was characterized by improvements in interlimb coordination. These improvements were completed quickly (by the end of Day 1) and were accomplished by the engagement of a particular type of corrective movement involving only the forepaws. The second phase developed on an intermediate time scale (Days 2–5), and was characterized by changes in intralimb stepping: mice gradually shortened the lengths of individual strides, such that they took shorter strides more frequently. The final phase began around Day 6 of training, after all mice had mastered the task and were able to successfully maintain balance on the wheel through trial completion. In this late phase, mice directed their stepping across paws to effectively drive body position back and forth on the wheel. This led to an increase in the variability of some metrics of kinematics but not others, and suggests the development of motor skill.

Collectively, our findings reveal that locomotor learning proceeds in distinct phases characterized by distinct corrective adjustments. These results present a new experimental platform for studying motor learning with high spatial and temporal precision that will facilitate future studies into the circuit and plasticity mechanisms supporting skill development.

## EXPERIMENTAL PROCEDURES

Male and female heterozygous mice on a C57BL/6J background ($N$ = 7 mice; 3 male; 4 female; 18–27 g; 10–11 week old) were used for these experiments. Mice were housed in standard home-cages (2–4 animals per cage) on a reversed 12 hour light/12 hour dark cycle with *ad libitum* access to water and food. All procedures were carried out in accordance with the National Institutes of Health guidelines and with the approval of the Institutional Animal Care and Use Committee of Carnegie Mellon University.

### Experimental design

*Wheel setup.* The RotaWheel is a new experimental platform for assessing paw and body kinematic changes during a locomotor skill learning task in mice (Fig. 1A). Two 3D printed wheels (2 inch (5.08 cm) diameter, 0.5 inch (1.27 cm) wide, positioned 0.25 inches (0.635 cm) apart) are supported 7 inches (17.78 cm) from the ground, and are driven by two separate motors. A clear acrylic panel on either side of the wheel prevents the mice from climbing off. The speed of each wheel is independently programmable using an Arduino-operated DC motor and a custom-programmed proportional-inte gral-derivative (PID) feedback control loop operating at 20 Hz. Mice are imaged using two high-speed cameras placed on either side of the mouse, approximately 50 mm away at the same horizontal plane of the wheel, to obtain lateral views of paw and body motion. The cameras (Basler ace, acA800-510uc) operate at 100 frames per second (fps) (max 511fps) with a 832 $\times$ 632 pixel resolution. Stable lighting conditions were maintained with cool white light lamps, and UV lights were used to maximize body and paw contrast. A white LED visible to each camera was used to sync video frames from the left and right side for each experimental trial.

*Wheel training.* Mice were trained on the wheel for 14 consecutive days. Each training day began with a static 15 rpm running protocol which lasted for 30 s. Following this initial trial, mice were exposed to 80 s accelerating ramp trials (in which the speed increased linearly from 10 to 50 rpm or 2.66 to 13.30 cm/s) interleaved with 15 s static trials of varying speeds (20, 25, 30, 35, or 40 rpm), for a total of 11 trials per day. Analysis was restricted to only the 5 accelerating ramp trials. Animals were required to walk on the wheel for at least 5 s for the trial to be valid. If mice could not keep up with the driven wheel speed, a clear acrylic wall placed just below the bottom of the wheel prevented mice from hanging on the wheel and making full rotations. After each trial, mice were held in a small, enclosed box for 5 minutes to rest and minimize off-wheel locomotion. After training, mice were returned to their home cage.

### Data acquisition

We designed an automated paw tracking algorithm to extract the position of each paw and the body center of the mouse at 100 frames per second. Tracking and analysis of body and paw data was performed offline using custom Matlab code. All code used for the data collection and analysis, along with associated design files, are available at the following GitHub repository (https://github.com/katpnug/RotaWheel).

Before applying the paw-tracking algorithm, we performed camera lens distortion correction using Matlab's Camera Calibration App through the Computer Vision Toolbox. The paw tracking algorithm involves two steps: image segmentation and paw classification. These steps are described in detail below.

*Image segmentation.* To increase paw contrast and aid in paw tracking, at the start of each day's training we colored each paw with a fluorescent marker: green for the front left and hind right, and orange for the front right and hind left, as these colors are easily distinguished. To extract paw position, every camera frame is processed in the following way.

First, we applied a decorrelation stretch to each image frame, to minimize the cross correlation between different color bands, effectively performing signal whitening. We then applied color thresholds to each frame to identify green and orange pixels (paws), and dark brown pixels (body). Once clusters of each pixel color were detected, we performed morphological erosion and dilation image processing operations to create segmented objects, using built-in Matlab functions. Candidate paw and body objects were refined by removing objects which had fewer than 50 (front), 200 (hind), or 10,000 (body) connected pixels (*bwareaopen*). All remaining objects

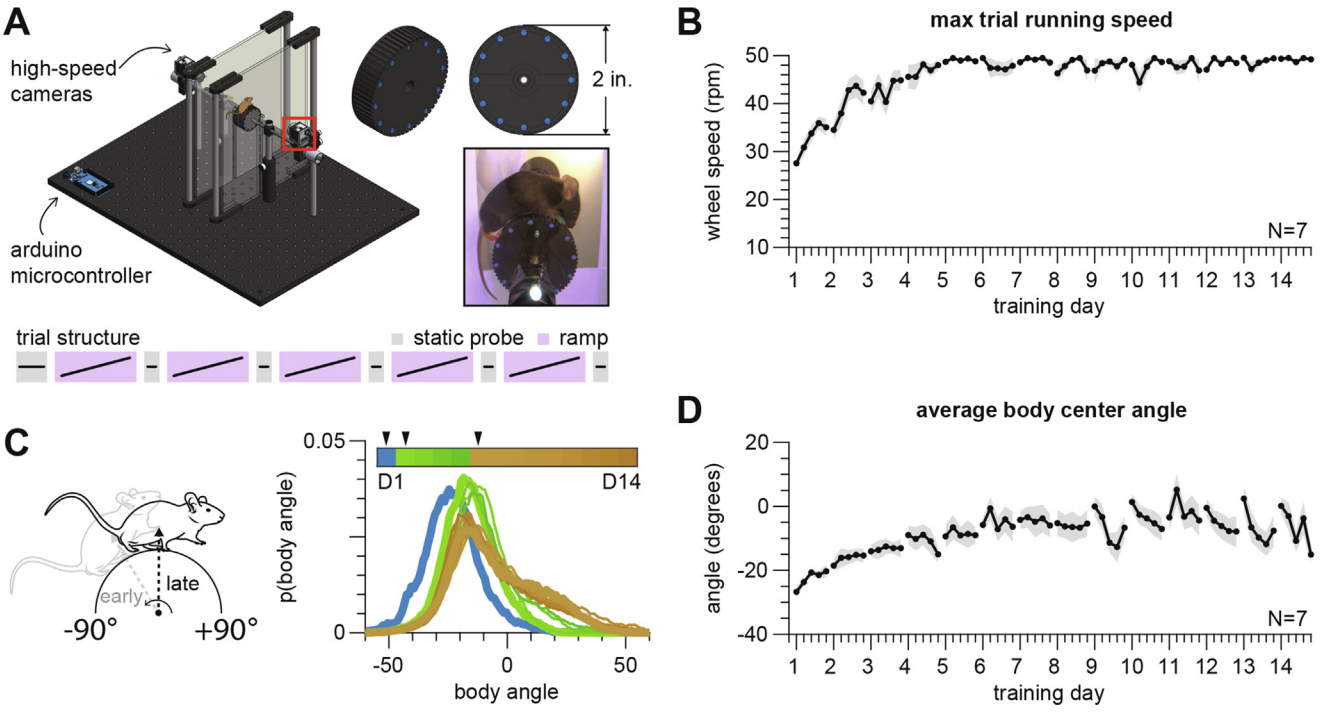


**Fig. 1.** Mice improve overall behavior on custom accelerating wheel. **(A)** Running wheel apparatus. Elevated wheels are controlled by a microcontroller. Two high-speed cameras capture side views at 100 fps. Bottom schematic illustrates training trial structure per day. 5 ramp trials highlighted in purple boxes were used to assess motor skill learning and paw kinematic changes. **(B)** Speed at fall performance in mice over 14 consecutive days of training ($N = 7$) on accelerating wheel. **(C)** Distribution of body center angle with respect to wheel center across training days. Black triangles represent the start of the three learning phases (early, intermediate, late). Statistical significance was assessed by a two-sample F-test for equal variances comparing Day 5 versus Day 6, and always showed $p < 0.01$ for each mouse. **(D)** Mean body angle across trials and days of training. A t-test for each mouse comparing Day 1 to Day 2 always showed $p < 0.001$. A t-test for each mouse comparing body center for Day 5 to Day 6 always showed $p < 0.001$. Data and shading represent mean ± SEM.

were then dilated using a flat, square structuring element with width 3 to expand and smooth feature edges for improved paw and body approximation (*imdilate*). Finally, we defined a rectangular bounding box around each connected blob object candidate. We only ever detected a maximum of one object for body center. However, segmentation can return multiple putative paw objects per frame. Thus, we solve the data assignment problem of classifying each detected object using an iterative Bayesian procedure, described below.

*Classification.* First, we defined Gaussian probability distributions over each paw's x- and y-position, as well as the paw area using hand-labeled data described below. Separate distributions were defined for front and hind paws. Then, for each image frame we computed the likelihood of each putative paw object under those distributions as:

$$\underset{class}{\operatorname{argmax}} \left[\log P(centroid|class) + \log P(area|class)\right] \quad (1)$$

where class can be front or hind. Note that we treated paw area as independent of the x/y paw centroid position. Each observation returns a likelihood value for the front and hind class, which is then ranked and labeled based on maximum likelihood. Since only certain combinations of labels can exist per frame, an iterative process finds the maximum of any repeated paw labels and rejects remaining bounding boxes as noise. This process ensures that, in each frame, there can only be one front paw and one hind paw object. Furthermore, the front paw can never fall in a position behind the hind paw.

In the final step, we evolved the paw probability distributions over time. Our ad-hoc procedure works as follows. First, we quantified the certainty of the classification for this frame as the log-likelihood of the centroid/area data (the value inside the argmax function of Eqn. (1)). If this value was greater than 25, we deemed the classification as certain (the value 25 was found in cross-validated hand-labeled data to give the best tracking performance). When labeling was certain, we updated the mean of the prior distribution to the current centroid $\left(\mu_t = \begin{bmatrix} x \\ y \end{bmatrix}\right)$ and covariance to the width and height $\left(\sum_t = \begin{bmatrix} width & 0 \\ 0 & height \end{bmatrix}\right)$ of the observed bounding box. Otherwise, if flagged as uncertain, the distribution began to decay towards the original steady state parameters from the hand-labeled frames (Equation (2)).

$$\mu_t = \alpha(\mu_{t-1} - \mu_{ss}) + \mu_{ss}, \ where \ \mu_{ss} = \begin{bmatrix} \overline{x_{ss}} \\ \overline{y_{ss}} \end{bmatrix}$$

$$\sum_t = \alpha\left(\sum_{t-1} - \sum_{ss}\right) + \sum_{ss}, \ where \sum_{ss} = \begin{bmatrix} \sigma^2_{x_{ss}} & \rho\sigma_{x_{ss}}\sigma_{y_{ss}} \\ \rho\sigma_{x_{ss}}\sigma_{y_{ss}} & \sigma^2_{y_{ss}} \end{bmatrix} \quad (2)$$

The decay rate alpha was set to 0.75.

### Interpolation

For any missing data, paw positions were linearly interpolated in x/y-coordinates using existing data which flanked the missing points. If data was missing at the very beginning or end of a trial, no points were interpolated. Points that were interpolated at the transition between a swing and stance phase (e.g., around a trough or peak of the angle trace) were discarded. Interpolation was used on 2.26% of points across all data frames.

### DeepLabCut

We also trained a model using the DeepLabCut toolbox to estimate the positions of the front paw, hind paw, body center, and wheel center. A total of 200 image frames (10 videos, 20 frames/video) were used to label and train the model. A pre-trained network with 50 layers (ResNet50) was selected and trained for 500,000 iterations, where the cross-entropy loss plateaued to ~0.001.

### Hand labeling

To fit prior distributions and assess the efficacy of our tracking algorithm, we hand-labeled a representative trial of wheel running from a static 40 rpm running trial. A total of 300 hand-labeled frames (15 s, 100 fps, left and right side) were imported into Matlab's Training Image Labeler application to manually insert rectangular bounding boxes for the front and hind paw of each frame.

This set of ground truth labeled data provided two unique features for the front and hind paws. First, the front and hind paws have distinct mean centroid x- and y-position coordinates. Second, the average area of the paw bounding boxes is markedly different, with the front being smaller than the hind paw. Using the heuristics discovered from the ground truth dataset, steady state Gaussian distributions for bounding box centroid position ($x_{ss}$, $y_{ss}$) and area ($a_{ss}$) were constructed to initialize parameters for automated paw classification.

### Body and paw kinematics estimation

We extracted several parameters from the body and paw kinematic data to assess performance and track behavioral adjustments during learning. The data are described as angles with respect to the wheel's rotational axis.

*Max trial wheel speed.* We determined the time of fall, if it occurred, by determining when the mouse body center fell further back on the wheel than −80 degrees. We determined through a sample of videos that mice never recovered from this position. The corresponding wheel speed was marked as the maximum wheel speed obtained on that trial.

*Speed bins from ramp trials.* Results reported here are only from the accelerating ramp trials. To examine any speed-dependent effects on paw kinematics, the 80 s trial was subdivided into six different speed bins. Each bin contained 20 s of data, where the average driven wheel speeds were 15, 20, 25, 30, 35, and 40 rpm, each with a range of +/− 5 rpm. Unless otherwise indicated, results are shown from the 15–25 rpm speed range (20 rpm bin). Note that each speed bin contains overlapping data. For example, the 20 rpm bin (15–25 rpm) and 25 rpm bin (20–30 rpm) share the same data between 20 and 25 rpm. We do this to ensure that we have enough paw strides per bin. This lower speed range was specifically chosen for analysis because mice were able to maintain wheel running within this range even on Day 1 Trial 1.

*Interlimb coordination parameters.* To evaluate interlimb coordination, we examined how a paw's movement was related to the other paws. Here, a stride is defined as a single complete cycle of a paw, from one footfall to the next footfall. Within a stride, the stance phase is the interval of time from the initial footfall to liftoff (i.e., when the paw is on the wheel, riding backwards). The swing phase is defined as the latter half of a cycle, where the paw is off the wheel moving forwards (from liftoff to footfall).

Based on each paw's stance and swing phase, we examined the gait by determining the percentage of time each mouse had 1–4 paws on the wheel. To examine finer coordination patterns, we performed a phase analysis to quantify the order and timing of footfall of all paws with respect to a reference paw (hind right). The footfall timing was reported as occurring at a percentage of the phase of the reference paw (from 0, synchronized to the reference paw's initial footfall, to 100, synchronized with that paws final footfall).

During some cycles, the forepaws made noticeable pauses in the forward movement while off-wheel, an action we term a "hover". We quantified the timing of the hover by analyzing the paw angle during the swing phase on each cycle. We first used a Matlab built-in function (findchangepts) to detect abrupt changes in the paw angle during the swing. The function was set to detect linear changes (i.e., changes in the slope of the paw angle as a function of time) with two as the maximum number of significant changes. The function returned the indices of significant changes in angle velocity. To estimate the hover time, we linearly extrapolated the initial paw angle velocity trace forward in time to identify when it intersected the actual footfall paw angle. The time difference between the extrapolated intersection and the actual footfall was defined as the hover time (see Fig. 4 for details). To classify hover and non-hover cycles, we fit a Gaussian mixture model to the distribution of hover times on data from Day 1 Trial 1 from all mice at the 20 rpm bin speed. The distribution model was fit with 2 components and the EM algorithm was repeated 100 times. This method returned a hover threshold of 0.034 s, where any cycles which had a smaller value were classified as non-hover and any cycles which had a larger value were classified as hover cycles.

*Intralimb parameters.* As changes in kinematics can be made to each paw independently without affecting across-paw coordination, we also identified intralimb parameters: stride length, cycle frequency, and duty factor. The stride length was calculated as the arc length (with wheel diameter = 2 in.) during the off-wheel swing phase. The cycle frequency was calculated as the inverse of the cycle duration (footfall-to-footfall or stance duration + swing duration). Duty factor was defined as the ratio of the stance duration to the cycle duration.

*Curve fitting.* To compare how the three phases of learning evolved with training, we fit curves to data representing each. Matlab's *fitoptions* with the *fit* function was used to define the fitting options. Specifically, an exponential fit of the form $y = a * e^{-\frac{x}{t}} + b$ was used to fit the max speed at fall, hover time, and swing length learning curves. A nonlinear least squares fitting method was used, with the lower bound of the $t$ coefficient constrained to 0. For stride mismatch, a sigmoid function of the form $y = a + (b - a)/(1 + 10^{(c-x)*d})$ was fit to the data using the *sigm_fit* function with no fixed parameters and automatic initial parameters. Finally, each curve was normalized to start at 0 and scaled so that the max value of the curve equaled 100 to compare the different phases.

### Statistical analysis

Offline statistical data analysis was done in MATLAB. To test for equal variances between two distributions, we used a two-sample F-test. Circular statistics were used to test for significant changes in mean values for circular phase plots (Circular Statistics Toolbox, Matlab). Paired and unpaired t-tests were used to test for statistical significance between groups or between training trials. To quantify changes in variability, we grouped all the data when variability was at its minimum (Days 2–5) and compared this mean and variance to other training time points with unpaired t-tests. The level of significance was $p < 0.05$ for all datasets and data is represented as means ± SEM unless otherwise noted.

## RESULTS

To characterize the kinematic strategies which underlie locomotor skill learning in mice, we designed the RotaWheel, a novel motorized running wheel in which body and paw kinematics can be tracked with high-speed cameras (Fig. 1A). RotaWheel has several benefits for kinematic analysis during learning, including: (1) clear acrylic side panels for side filming to capture paw movements; (2) a modular design that enables the 3D printed wheel to be easily swapped out for a different sized wheel or surface texture; (3) open-source electronics that are affordable and offer flexible programming; and (4) programmable output pins (on Arduino microcontroller) to synchronize with other systems. The running wheel is similar to a rotarod (Jones and Roberts, 1968; Costa et al., 2004), but with a slightly larger diameter (2in., as opposed to the standard 1in.). Healthy control mice ($N$ = 7, 4 females) were trained to run on top of this elevated wheel as it accelerated from 10 to 50 rpm (2.66 to 13.30 cm/s) over the course of 80 s. To stay on the wheel, mice needed to adjust their locomotion to match the driven wheel speed. Each mouse performed 5 of these ramp trials per day for 14 consecutive days.

Mice learned to complete the task within the first four to five days of training, mirroring learning curves observed with the rotarod (Fig. 1B). As mice became more proficient at the task, their body position shifted forward on the wheel (Fig. 1C-D), recapitulating a second feature of learning observed with the rotarod (Cao et al., 2015). This behavior remained true even when separating the body center data into speed bins to control for running wheel speed (Supp. Fig. S1). Analysis of body angle over time revealed three phases of behavioral performance: early, intermediate, and late (Fig. 1C; black triangles). On the first day of training ('early'), mice struggled to stay on top of the wheel, as reflected by a body center angle that was more negative than on subsequent days (Fig. 1C, D; a t-test for each mouse comparing Day 1 to Day 2 always showed $p < 0.001$). Over the next 4–5 days ('intermediate'), mice shifted their body position more forward on the wheel and learned to complete the task (Fig. 1B–D). Finally, with extended practice (beginning Day 6, 'late'), mice began to move their body position back and forth on the wheel, maintaining an average forward body position, but with greater variance (Fig. 1C, D; a t-test for each mouse comparing body center for Day 5 to Day 6 always showed $p < 0.001$; a two-sample F-test for equal variances for each mouse comparing Day 5 vs Day 6 always showed $p < 0.01$).

To examine changes in paw coordination and kinematics that accompany locomotor learning on this task, we performed video analysis of the front and hind paw positions using custom-built tracking algorithms (Fig. 2A). We assessed the accuracy of our algorithm by comparing its output to the paw positions of a representative 30 s video that was hand-labeled (Fig. 2B; solid curves). Our algorithm returned labeled paw data in 93.8% of frames, and produced an accurate estimate of the paw's location on 99% for forepaws and 98% for hind paws in those frames, as verified on cross-validated hand-labelled data (see Methods and Supp. Fig. 2A for more details). Comparison of paw centroid angles to the widely used DeepLabCut tracking algorithm (Mathis et al., 2018) revealed similar output, although our custom method returned points that were closer to the hand labeled dataset, on average (Supp. Fig. S2B).

### Interlimb coordination is refined during early learning

To investigate possible changes in interlimb coordination during learning, we first performed a gait analysis. We speculated that mice might eventually switch from walking to trotting on the wheel at higher speeds. This is not what we observed. In fact, we found that mice used a walking gait across the range of speeds we tested. Across all speeds, three paws were simultaneously in

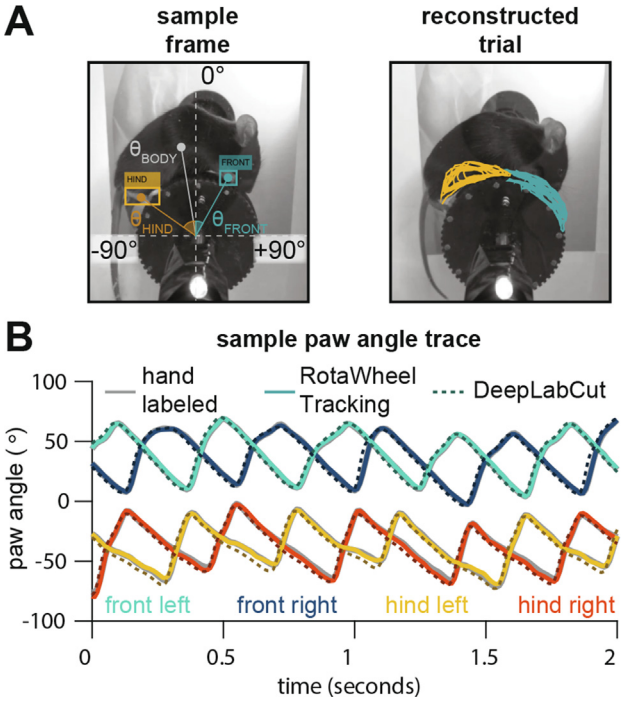


**Fig. 2.** Paws can be tracked and classified with precision. **(A)** Classified front and hind paw bounding box for one frame. Schematic shows position of paws represented in angles with respect to the wheel center (left). Sample trial paw trajectory traces (right). **(B)** Two second trace comparing hand-labeled (grey), RotaWheel tracking (solid colored), and DeepLabCut (DLC) (dashed colored) paw angles.

contact with the wheel for the majority of time, which is the signature of a quadruped walking gait (Hildebrand, 1965; Bellardita and Kiehn, 2015). Moreover, the same lateral sequence walking gait was maintained throughout wheel training (Fig. 3A, B).

We next investigated if mice changed how their limbs were coordinated within this walking gait. We define a gait cycle as the time between two sequential footfalls of a reference paw. We used the hind right paw as the reference because of its relative stability throughout learning, but our results do not change when other paws are used as the reference. Mice completed roughly 125 cycles over the course of a full 80 s trial. To quantify inter-limb coordination, in each cycle we computed the phase of each paw's footfall with respect to the footfall of the reference paw (Bellardita and Kiehn, 2015) (Fig. 3B, C).

Changes in interlimb coordination were observed on Day 1. On the first trial, mice walked with a gait where footfalls occurred at evenly distributed times within the cycle (Fig. 3D). That is, a paw touched down onto the wheel at roughly every 25% of a cycle (Fig. 3D, left). As mice performed more trials, the coordination of footfalls shifted and became more stereotyped across mice: the timing between footfalls of diagonal paws was shortened whereas the timing between contralateral paws stayed the same, creating a more asymmetric footfall distribution over the cycle (Fig. 3D, right). Relative to the hind right paw, the diagonal front left paw shifted from 77 ± 12% on Trial 1 to 89 ± 4% on trial 5 ($p$ = 0.02, circular test for significance of the mean), while the contralateral hind left paw did not change significantly ($p$ = 0.45, circular test for significance of the mean). These changes in coordination were accompanied by a decrease in the variance of footfall timing, suggesting an increase in precision (Fig. 3E). The diagonal footfall variance decreased from 0.06 on Day 1 Trial 1 to 0.03 on Day 1 Trial 5 ($F$(145,152) > 1, $p$ < 0.01, two-sample F-test), and the contralateral footfall variance showed a decrease from 0.06 on Day 1 Trial 1 to 0.02 on Day 1 Trial 5 ($F$(128,158) > 1, $p$ < 0.01, two-sample F-test).

The above shift in footfall timing and decrease in variability were analyzed on cycles when the average wheel speed was 20 rpm (range 15–25 rpm). To determine whether changes in paw coordination were robust across all speeds tested, we repeated these analyses on cycles taken from six different average wheel speeds (15–45 in 5 rpm increments, see Methods). Similar changes in timing and precision of diagonal paws were observed at all speeds, though the

**Fig. 3.** Interlimb coordination shifts with training. **(A)** Percentage time a certain number of paws are on the wheel on Day 1 early in training (left) and Day 14 late in training (right). **(B)** Representative schematic aligned to one full cycle of the hind right paw (orange). Solid colored and white lines indicate when each paw was on (stance) and off (swing) the wheel, respectively (bottom panel). Vertical dashed lines mark the touch-down point of each paw. **(C)** Order of paw touch-down events when aligned to the hind right paw (orange). **(D)** Circular phase plots with the mean touch-down point of the front left (teal), front right (blue), and hind left (yellow) paws aligned to the hind right (orange, reference paw) cycle. Phase plots show the average phase across mice (large circles) as well as data from individual mice (small circles). Phase plot statistical significance was assessed by circular test for significance of the mean of trial 5 compared to trial 1. Diagonal front left paw Day 1 Trial 1 versus Trial 5: 77 ± 13% on Trial 1 to 89 ± 4% on Trial 5, $p$ = 0.02. Contralateral hind left paw Day 1 Trial 1 versus Trial 5: 55 ± 18% on Trial 1 to 53 ± 7% on Trial 5, $p$ = 0.45. Ipsilateral front right paw Day 1 Trial 1 versus Trial 5: 34 ± 4% on Trial 1 to 42 ± 2% on Trial 5, $p$ = 0.02. **(E)** Histograms of all cycles (left) for diagonal (Day 1 Trial 1, $n$ = 146 cycles; Day 1 Trial 5, $n$ = 153 cycles) and contralateral (Day 1 Trial 1, $n$ = 129 cycles; Day 1 Trial 5, $n$ = 159 cycles) pairs. Box plots (right) show Day 1 Trials 1 versus 5 for diagonal and contralateral paw pairs. Data shown for 20 rpm speed bin during Day 1 Trial 1 and Trial 5. Statistical significance was assessed by circular test for significance of the mean. A two-sample F-test for equal variances also assessed variance of the footfall time differences between Day 1 Trial 1 and Day 1 Trial 5. Diagonal $\sigma^2$ Trial 1 = 0.06, $\sigma^2$ Trial 5 = 0.03, F(145,152) > 1, $p$ < 0.01. Contralateral $\sigma^2$ Trial 1 = 0.06, $\sigma^2$ Trial 5 = 0.02, F(128,158) > 1, $p$ < 0.01. **(F)** Average phase values for each speed bin (left) and standard deviation of phase for each speed bin (right) for Day 1 Trial 1 (dark) or Trial 5 (light). Statistical significance was assessed by a circular t-test comparing Trial 1 to Trial 5 for each speed bin. **(G)** Average phase values at 20 rpm across all training trials and days for diagonal and contralateral pairs. Statistical significance was assessed by a circular statistics comparing Day 1 Trial 1 to each training trial. Points with $p$ < 0.05 are indicated with filled colored markers.

effect was smaller as speeds increased (Fig. 3F). Note that it is difficult to make comparisons in the 35 and 40 rpm speed bins on Day 1, as many mice did not complete those speeds on the first day.

Finally, we analyzed the time course of interlimb coordination changes (Fig. 3G). Changes in diagonal coordination were completed by the end of Day 1 and were retained across subsequent days of testing. Thus, changes in interlimb coordination occur quickly and are maintained throughout the duration of experience.

### Changes in paw coordination may be mediated by a corrective 'hover' step

To determine how mice adjust their paw coordination, we analyzed their stride kinematics. Stride timing can change due to differences in paw liftoff time, paw touchdown time, or both. We first examined liftoff time. Training had no effect on the diagonal lift-off time difference (Supp. Fig. S3A-B).

We next examined footfall timing. On the first trial, the majority of strides had smoothly accelerating and decelerating paw velocities during the swing phase (as paws are moving forward in the air; Fig. 4A top and Fig. 4B left column). However, with training, an increasing number of strides were observed with a biphasic deceleration phase, in which paws 'hovered' just before being placed back down on the wheel (Fig. 4A bottom, Fig. 4B right, and Supp. Video S1). We computed this hover time as the time between when the foot would have touched the wheel without slowing, versus when it actually touched the wheel. There was a bimodal distribution in the hover time, suggesting that mice either hover or do not on any given stride (Fig. 4C). Hover was only ever observed in the forepaws.

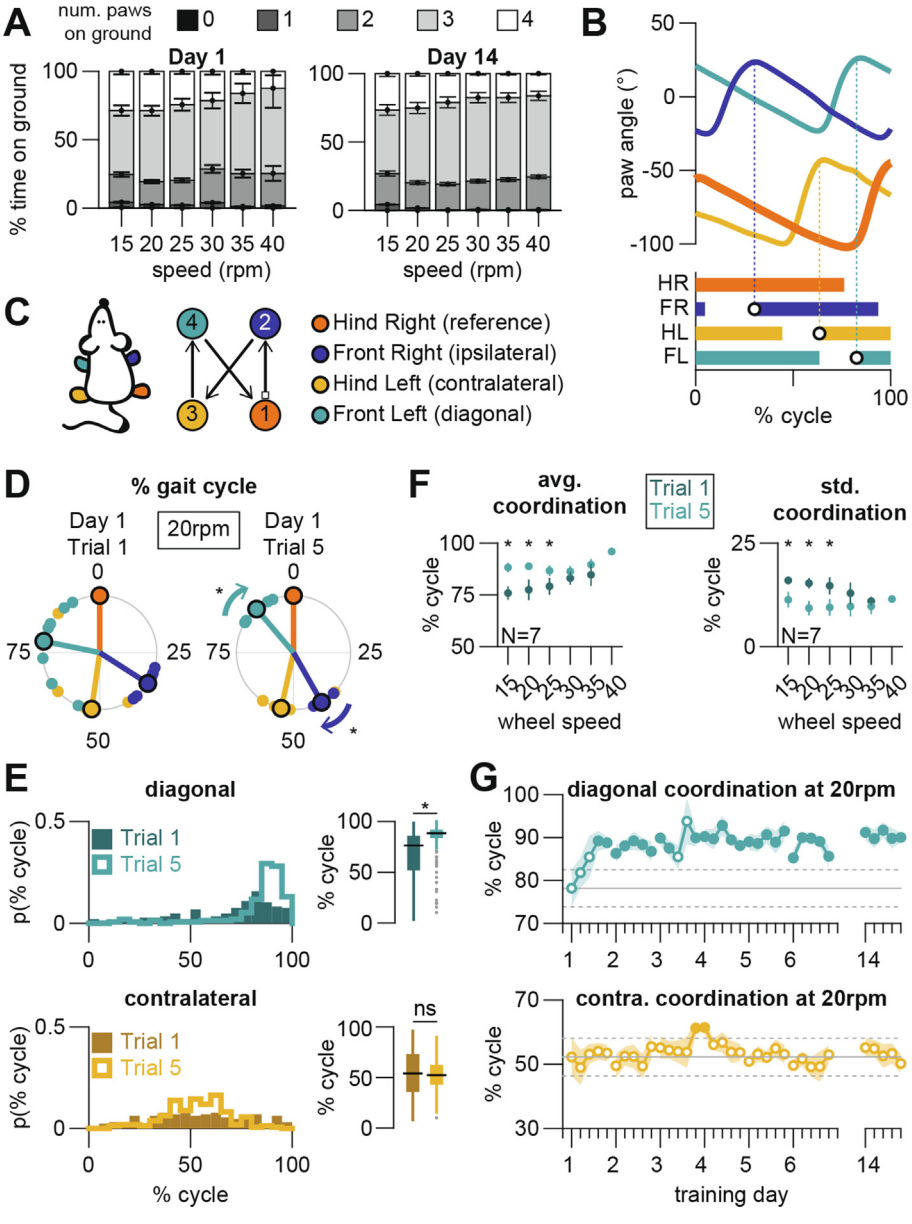


Hover strides became more pronounced during the first day of training. We classified hover and non-hover steps using a Gaussian mixture model. Over the course of Day 1, we observed an increase in both the proportion of hover strides (Fig. 4D, top; Trial 1: 0.53 ± 0.09, Trial 5: 0.77 ± 0.13, $p$ = 0.002), as well as the duration of the hovers themselves (Fig. 4D, bottom; Trial 1: 0.08 ± 0.01 s, Trial 5: 0.13 ± 0.02 s, $p$ = 0.0002). This remained true even when we controlled for body center position across training days by restricting analysis of hover strides to only when the mouse was slightly towards the back of the wheel (Supplemental Fig. S3C). The time course of hover changes paralleled the time course of paw coordination changes described in Fig. 3; hover increased rapidly during Day 1, but then remained relatively stable across subsequent days of training (Fig. 4D).

We hypothesized that the hover stride might be a "corrective" movement used to shift the coordination of the diagonal paws. To test this hypothesis, we computed the time differences between diagonal footfalls on all strides, and compared this to the predicted time differences that would have occurred without hover (Fig. 4E). On Day 1 Trial 1,

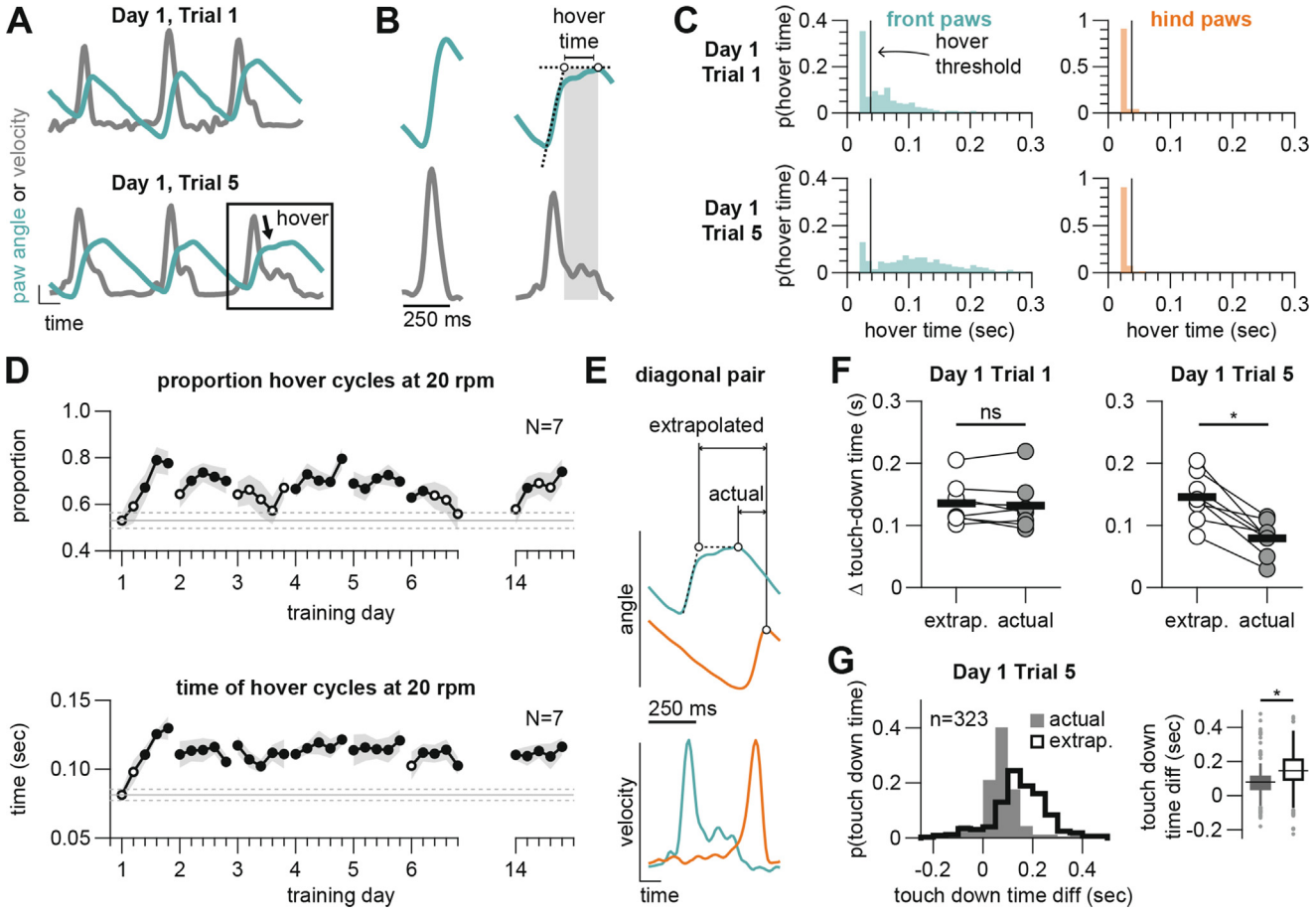


**Fig. 4.** Stride swing timing drives interlimb coordination changes. **(A)** Sample paw angle (teal) and corresponding velocity (grey) traces of one mouse for Trial 1 (top) versus Trial 5 (bottom) and Day 1 of training. Black arrow points to change in paw velocity mid-swing. **(B)** Sample swing cycle paw angle and velocity curves for non-hover (left) and hover (right). Schematic illustrates quantification of hover time using change in paw angle slope. **(C)** Histogram of hover time for front (left) and hind (right) paws of all cycles across all animals for Day 1 Trial 1 (top row) and Trial 5 (bottom row) at 20 rpm speed bin. Vertical line indicates hover threshold determined from Trial 1 data. **(D)** Average proportion of hover cycles and hover time for classified hover cycles in forepaws as a function of training. Proportion of 1 is 100% of cycles in 20 rpm bin. Mean ± SD across animals. Statistical significance was assessed by t-tests comparing Day 1 Trial 1 to each subsequent day and trial. Points with $p < 0.05$ are indicated by black filled markers. Solid horizontal line denotes mean and dashed line is SEM of animals ($N = 7$) from Day 1 Trial 1. **(E)** Schematic showing difference in actual versus extrapolated (if there was no hover) touch-down time between the diagonal paw pair of one cycle. **(F)** Paw touch-down time difference between extrapolated and actual on Day 1 Trial 1 (left) and Trial 5 (right). Thick horizontal line represents mean of 7 animals. Statistical significance was assessed by t-tests. Extrapolated: 0.14 ± 0.04, actual: 0.13 ± 0.04, $p = 0.54$. No-hover prediction: 0.15 ± 0.04, actual: 0.08 ± 0.03, $p = 0.003$. **(G)** Histogram shows touch-down time difference probabilities of actual (filled) and extrapolated (outlined) times for all cycle data on Day 1 Trial 5. Box plot (right) shows median and spread of touch-down time difference between actual and extrapolated times. Statistical significance was assessed by t-tests. Actual: 0.08 ± 0.005, extrapolated: 0.14 ± 0.006, $p < 0.01$. A two-sample F-test for equal variances assessed variance of the footfall time differences between actual and extrapolated. $\sigma^2_{\text{actual}} = 0.007$, $\sigma^2_{\text{extrapolated}} = 0.01$, $F(322,322) > 1$, $p < 0.01$.

there was no significant difference between the no-hover predictions and actual footfall time differences of the diagonal paws (Fig. 4F, left; extrapolated: 0.14 ± 0.04, actual: 0.13 ± 0.04, $p = 0.54$). On Day 1 Trial 5, when hover times peaked, the actual footfall time difference was significantly less than the no-hover predictions (Fig. 4F, right; no-hover prediction: 0.15 ± 0.04, actual: 0.08 ± 0.03, $p = 0.003$). Additionally, the distribution of the actual footfall time difference for all strides across mice was less variable than that of the no-hover predictions (Fig. 4G; $\sigma^2_{\text{actual}} = 0.007$, $\sigma^2_{\text{extrapolated}} = 0.01$, F(322,322) > 1, $p < 0.01$, two-sample F-test). Thus, it appears that mice regulated their interlimb coordination using timed pauses in the forelimb swing to increase the interlimb temporal precision of footfalls.

## Stride length decreases gradually across multiple days of training

Thus far, we have shown that rapid behavioral improvement on Day 1 is well correlated with adjustments in interlimb coordination. But after Day 1, behavioral performance continued to improve, whereas interlimb coordination metrics remained constant. This suggests that other factors with slower time courses accompany improvement after Day 1.

Stride length has been shown to correlate with movement speed in both humans and animals (Reisman et al., 2007; Bellardita and Kiehn, 2015; Machado et al., 2015; Lemieux et al., 2016). To study whether mice adjusted their strides with experience, we analyzed the swing length, defined as the circumferential distance a

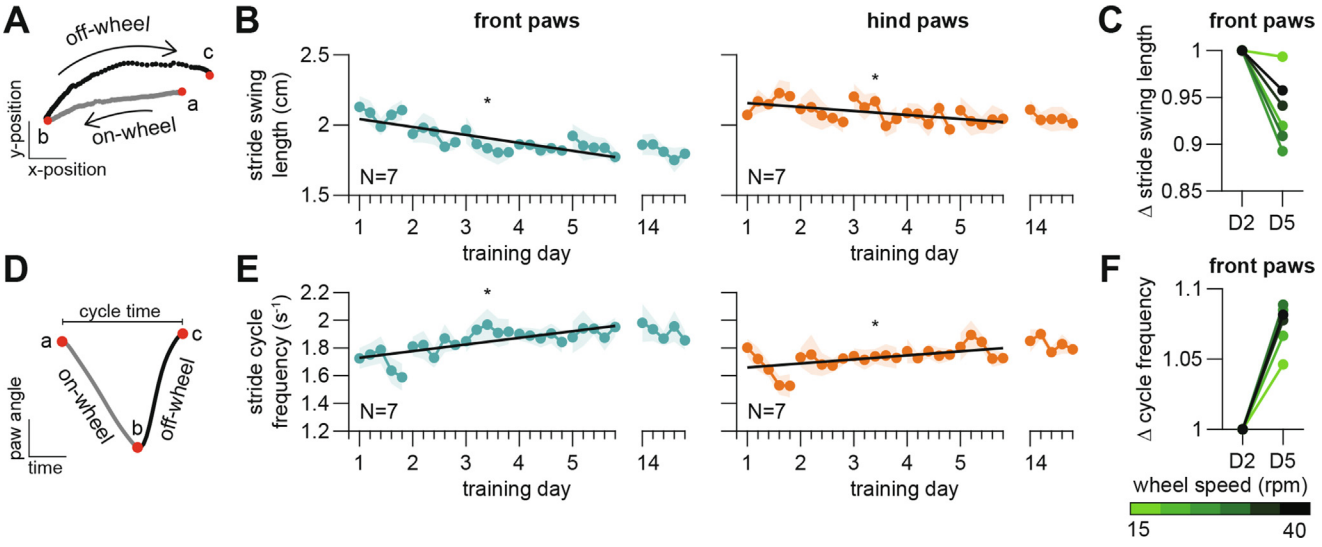


**Fig. 5.** Slow changes are present in intra-limb metrics. **(A)** Schematic of stance (on-wheel) and swing (off-wheel) phases for one cycle. **(B)** Stride swing length for front (left) and hind (right) paws across training days for 15–25 rpm speed range (20 rpm bin). Black curve shows a least-squares fit linear regression of the form $y = \beta_0 + \beta_1 x$ from Days 1–5. Front swing length: $p < 0.01$, F-stat = 34.7, $R^2 = 0.17$; hind swing length: $p = 0.01$, F-stat = 6.55, $R^2 = 0.03$. **(C)** Change in swing length for all six speed bins normalized by Day 2 values. **(D)** Schematic depicting one cycle in paw angle across time. **(E)** Cycle frequency for front and hind paws across training days. Black curve shows linear regression of data from Days 1–5. Front frequency: $p < 0.01$, F-stat = 17.4, $R^2 = 0.09$; hind frequency: $p < 0.01$, F-stat = 8.48, $R^2 = 0.04$. **(F)** Change in frequency for all speed bins normalized by Day 2 values.

paw moved between consecutive footfalls (Fig. 5A; point b to c). Across training days, mice exhibited a gradual, significant reduction in the stride length of their forepaws (Fig. 5B). Because stride length appeared to be changing on a slower timescale, we wanted to compare the changes between Days 2 and 5. Looking at strides around 20 rpm (range: 15–25 rpm), the average stride length on all trials of Day 2 was 1.92 ± 0.23 cm, while on Day 5 it was significantly less (1.84 ± 0.24 cm, $p = 0.01$). Reductions in stride length were observed across all speed bins (Fig. 5C). The hind paws showed a mild reduction in stride length from Day 2 to 5, but it was not statistically significant (Supp. Fig. S4). Note that the left and right sides were grouped together for the front and hind paws because we observe no asymmetry in the strides (Supp. Fig. S4C).

We also examined a related measurement, stride frequency (Fig. 5D; see Supp. Fig. S4D for swing duration, stance duration, and duty factor). The frequency of strides for the forepaws and hind paws gradually increased over a similar time course (Fig. 5E), across all six speed bins (Fig. 5F). Thus, mice gradually took shorter, quicker strides with training on this task.

## Mice exhibit directed variability in strides after task mastery

We predicted that a motivation to reduce stride length with training might be to increase the precision of movements. With shorter strides, it may be easier to place the paw down at the same position on the wheel as the previous stride. To investigate this possibility, we defined stride mismatch as the angular difference between the start and end points of a paw for each cycle, and used this as a measure of stride precision. On any given cycle, a paw could end behind its original position ('undershoot'), in the same position as it started ('regular'), or end more forward than its original position ('overshoot') (Fig. 6A and Supp. Video S2).

If strides become more precise with training, we would expect to see a decrease in stride mismatch, leading to an increase in regular strides. Intriguingly, we observed an increase, not a decrease, in stride mismatch variance with training. In other words, strides appeared to become less precise with training. Stride mismatch variance increased most noticeably at the beginning of Day 6 of training, and was maintained from Day 6 throughout the remaining training days (Fig. 6B).

The finding that stride precision declined was surprising, given that mice were successfully completing the full 80 s trial by this time. We thus hypothesized that mice were actively driving these "mismatches" for exploration; i.e., purposefully using undershoots and overshoots to control their body position on the wheel. On Day 1, the stride mismatch throughout a trial was small and relatively flat (Fig. 6C, top; sample 50 strides shown at 20 rpm bin). By Day 6 of training, a rhythmic pattern of stride mismatch emerged, driven by consecutive large overshoots and undershoots across paws (Fig. 6C, bottom). Indeed, superimposing the body angle confirmed that the mouse's body center position followed the bouts of stride mismatches (Fig. 6C, grey curve). To further investigate this idea, we examined the correlation between a stride mismatch of one paw and the next paw that touched down for each trial. We observed an increase in correlation beginning around Day 6, indicating that mice were making similar mismatches in succession across two footfalls (Fig. 6D). Thus, mastery of the accelerated running wheel task was associated with increased variability in stride mismatches that directed

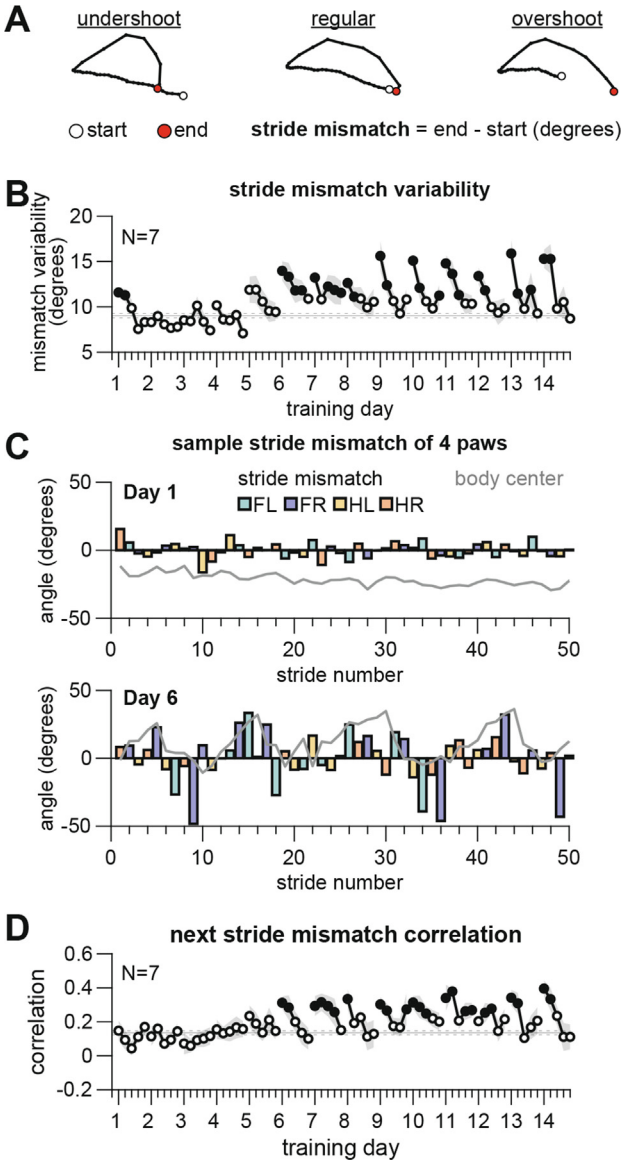


**Fig. 6.** Directed stride mismatches drives increases in body center variability. **(A)** Schematic illustrating three possible scenarios for stride mismatch (undershoot, regular, overshoot). **(B)** Stride mismatch variability across training days, reported as the standard deviation of stride mismatch. Grey shading represents standard error of the mean across animals. We compared mismatch variability when it was at its minimum (Days 2–5) to other training time points. Statistical significance was assessed by unpaired t-tests comparing each trial to the average of this minimum variability range (Days 2–5). Points with $p < 0.05$ are indicated by filled markers. Solid horizontal line dictates mean and dashed line is SEM of Days 2–5. **(C)** Stride mismatch of all 4 paws of 50 strides during a sample trial for Day 1 (top) and Day 6 (bottom). Grey curve represents the body center angle. **(D)** Average correlation value across training days of one paw to the next paw that touched down. Statistical significance is indicated as in B.

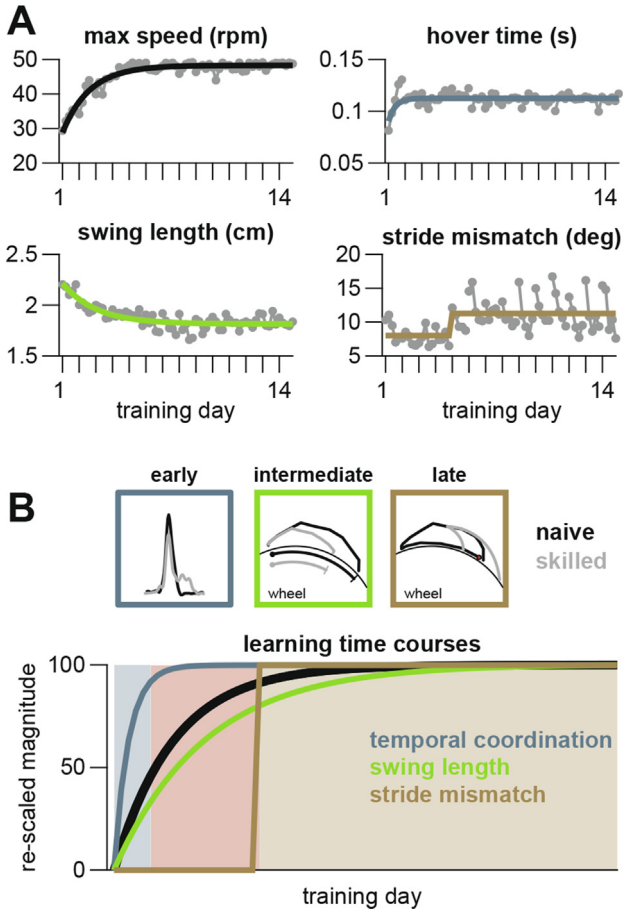


**Fig. 7.** Three phases of learning are present in a mouse locomotor learning task. **(A)** Fitted curves to data representing overall behavioral performance (max wheel speed reached), early phase (hover time), intermediate phase (swing length), and late phase (stride mismatch). An exponential fit of the form $y = a * e^{-\frac{x}{t}} + b$ was used for to fit the max speed at fall, hover time, and swing length learning curves. For stride mismatch, a sigmoid function of the form $y = a + (b - a)/(1 + 10^{(c-x)*d})$ was fit to the data. **(B)** Comparison of the rate of change of the 3 learning phases with overall performance (black). Each curve (from A) was normalized to start at 0 and scaled so that the max value equaled 100 to compare the different phases.

body position forward and backwards on the wheel, presumably for exploration. While the average variability increased, we noticed that there was also a consistent decrease in variability within training days, which we presume is due to fatigue across trials. As we speculate the increase in variability is a measure of how the mice explored the span of the wheel, fatigue would presumably decrease wheel exploration.

## DISCUSSION

While there is an ever-growing toolbox of neural engineering technologies that allow us to study and manipulate neurons at the single-cell level, an equally critical component for understanding the link between brain and behavior is the behavioral task itself (Krakauer et al., 2017). We designed the RotaWheel to study how locomotor kinematics and coordination patterns evolve with the development of locomotor skill. Collectively, our results show 3 distinct phases of behavioral changes as mice learn this skill (Fig. 7A). First, on Day 1, mice exhibit a fast change in interlimb coordination, mediated by a corrective hover step. From Days 2 through 5, mice gradually

change their intralimb stride length and stride frequency to make shorter strides more often. Finally, starting around Day 6, mice learn to direct the variability in their footfalls to explore the running surface, resulting in an increase in body center variability (Fig. 7B), without an increase in interlimb coordination variability (Fig. 3) or stride length variability (Fig. 5). These data provide further support for discrete changes in gait features that occur during a motor skill learning task in rodents, which has been previously observed in both rodent (Buitrago et al., 2004; Costa et al., 2004; Darmohray et al., 2019) and human (Bastian, 2008; Torres-Oviedo et al., 2011) studies. More importantly, we introduce a new experimental platform for detailed kinematic analyses during a motor learning task that will enable investigation of the circuit mechanisms supporting these learned changes.

### Corrective movements subserving changes in interlimb coordination

Mammalian quadrupeds have a flexible locomotor system, capable of executing distinct gaits to efficiently travel at different speeds and avoid obstacles (Hildebrand, 1965; Bellardita and Kiehn, 2015). It is well accepted that neural circuits in the spinal cord generate basic locomotor patterns to drive movement through the coordination of muscle activity across limbs. More recent studies suggest that there is a modular organization of these central pattern generators within the spinal cord for locomotion (Bellardita and Kiehn, 2015; Frigon, 2017). While the spinal cord has the architecture and plasticity to drive the behavioral kinematic changes observed throughout training, descending inputs from supraspinal structures are also likely to contribute to interlimb coordination and individual limb movements.

During the first day of training, mice learned to decrease the time and variability between diagonal footfalls. Interestingly, they accomplished this by implementing temporal pauses, or hovers, in the forepaws as they swung forward. The biphasic profile of the angular velocity observed in hover cycles closely resembles previous literature examining velocity profiles for eye saccades, which are presumably mediated by the cerebellum (Xu-Wilson et al., 2009). One hypothesis for the asymmetric movement velocities is an online internal feedback mechanism that corrects for variability (Shadmehr et al., 2010). In support of this idea, recent work in mice has identified the interposed nucleus of the cerebellum to enhance end-point reach precision, specifically by controlling limb deceleration (Becker and Person, 2019). Work by Darmohray and colleagues examining locomotor patterns during a split-belt adaptation task in mice also found that the interposed nucleus, and not the medial or lateral nucleus, is required for interlimb coordination adaptation, and the changes they observed were also mainly observed in the forepaws (Darmohray et al., 2019). Our data suggest that hovering is a within-cycle compensatory strategy that mice use to quickly adjust locomotor coordination and seems likely to be mediated by a similar cerebellar-dependent mechanism. However, we made assumptions that the reference hind paw would be unchanged in hover and non-hover strides as we needed a stationary reference for quantification. Thus, further dedicated experiments are needed to identify the exact role of hovers and pinpoint the neurological mechanisms driving this movement.

### Potential mechanisms of intralimb kinematic changes

Over several days of training, mice gradually learned to complete the trial by taking shorter, quicker strides. Why did mice adopt this strategy? While cardiovascular and muscular improvements are unlikely to be contributing to the fast interlimb changes, it is possible that the slower intralimb adjustments are a consequence of increased endurance and strength. However, studies which pre-exposed rodents to voluntary running wheels in the home cage prior to rotarod training have showed that this does not diminish the learning rate (Buitrago et al., 2004; Li and Spitzer, 2020). Thus, the kinematic changes observed on this task are likely due to a learned motor skill rather than increased fitness.

Locomotion is one of many examples where the motor system is tasked to choose a strategy by which it will achieve its end goal. The most efficient strategy not only depends on how all 4 paws coordinate with each other, but also how an individual paw moves. One prevailing optimal control model that explains typical motor behavior focuses on minimizing the impact of motor noise on generated movements (Harris and Wolpert, 1998). That is, there is a speed-accuracy tradeoff when executing goal-directed movements (Fitts, 1954). It could be that the changes in stride length we observe occur to minimize motor noise and lead to more robust control. Another possibility is that the changes in paw kinematics could be more effective in terms of metabolic cost required to maintain balance on top of the wheel.

If taking shorter and quicker strides produces more efficient movements, these adjustments could be mediated by the basal ganglia. Previous work in rodents have shown that the basal ganglia can modulate movement initiation, termination, and locomotor speed (Kravitz et al., 2010; Roseberry et al., 2016; Yttri and Dudman, 2016; Sales-Carbonell et al., 2018). Its direct projection to the mesencephalic locomotor region, which then communicates to central pattern generators in the spinal cord indirectly via relays in the reticular formation (Capelli et al., 2017; Caggiano et al., 2018; Josset et al., 2018) puts the basal ganglia in an ideal position to select the most appropriate stride length and frequency combination. Another possible explanation for these adjustments is that quicker, shorter strides enable better control of balance. The lateral vestibular nucleus has been shown to modulate flexor and extensor muscles which help offset perturbations to balance (Murray et al., 2018). Future studies employing circuit manipulations or examining how well mice adapt paw kinematics to abrupt speed transitions could help reveal the underlying mechanisms for these adjustments.

### Variability increases in some motor domains during skill learning

To our initial surprise, we found that stride mismatch, defined as the spatial difference between the start and end point of a footfall, increased with prolonged training. However, further investigation revealed that this variability was not random. Instead, mice learned to pattern their overshoot or undershoot strides in bouts to drive their body position on the wheel. Though this metric increased the variability of paw placement, it had no detrimental impact on task completion, as the mice were still able to complete the task. While skill acquisition is often linked to a decrease in variability, more recent studies suggest that variability and performance stability are independent, in that variability does not necessarily have to decrease to produce stable behavior. In fact, in complex dynamical systems, this can be a positive feature that allows for increased flexibility for the central nervous system to correct for perturbations (Wu et al., 2014; Sternad, 2018). The observed increase in variability may also reflect intentional exploration of the wheel surface.

This finding of increases in the variability of some metrics and not others suggests that RotoWheel learning is a skill as opposed to a habit. There are a few key differences in the hardware design and experimental protocol relative to the standard rotarod that might make the RotaWheel performance different in this regard. First, the larger diameter wheel gives mice the ability to explore the front or back of the wheel. Second, the accelerating profile used in this study allowed mice to fully complete the trial; something that does not happen in most rotarod studies. Both of these features may be more selective to skill learning rather than assessing maximal motor performance or endurance. Another group made similar design modifications to the rotarod (Shiotsuki et al., 2010). Using their larger diameter drum, they were able to identify motor learning deficits in Parkin-deficit mice compared to healthy controls which the standard small drum rotarod was unable to detect. It will be interesting in future work to determine the design criteria that lead to habit versus skill formation, and determine how various brain circuits contribute to each.

Locomotor skill learning proceeds through distinct phases associated with separable time courses and distinct behavioral adjustments. An initial fast acquisition period followed by a slow refinement phase has been reported in various mouse backgrounds and rats. Despite variability across strains and species, the preserved learning curve suggests the changes in kinematic adjustments reported in this study would generalize to other models. The presence of multiple timescales of learning parallels findings observed in humans (Smith et al., 2006; Joiner and Smith, 2008; Haith and Krakauer, 2013) and monkeys (Mandelblat-Cerf et al., 2011a, 2011b; Zhou et al., 2019) and implies the coordination of multiple learning circuits. The identification of specific locomotor adjustments in the RotaWheel task will allow for future motor learning studies to leverage the advanced genetic tools available in mice to dissect the neural circuits responsible for these learning processes.

## DECLARATIONS OF INTEREST

None.

## ACKNOWLEDGEMENTS

The authors would like to thank Gelsy Torres-Oviedo and Dulce Mariscal-Olivares for helpful discussions, and Jinke Liu and Nikhil Maheshwari for their contributions.

## AUTHOR CONTRIBUTIONS

**Katrina P. Nguyen:** methodology, data curation, analysis, writing, **Abhinav Sharma:** methodology, data curation, analysis, **Mauricio Gil-Silva:** analysis, **Aryn H. Gittis:** methodology, writing, review & editing, supervision, funding acquisition, **Steven M. Chase:** methodology, writing, review & editing, supervision, funding acquisition

## FUNDING

This work was supported by the Shurl & Kay Curci Foundation, NIH R01NS101016, NIH R01NS104835, and NSF IOS1553252.

## REFERENCES

Bastian AJ (2008) Understanding sensorimotor adaptation and learning for rehabilitation. Curr Opin Neurol 21:628–633.
Becker MI, Person AL (2019) Cerebellar control of reach kinematics for endpoint precision. Neuron 103:335–348.e5.
Bellardita C, Kiehn O (2015) Phenotypic characterization of speed-associated gait changes in mice reveals modular organization of locomotor networks. Curr Biol 25:1426–1436.
Brooks SP, Trueman RC, Dunnett SB (2012) Assessment of motor coordination and balance in mice using the rotarod, elevated bridge, and footprint tests. Curr Protocols Mouse Biol 2:37–53.
Buitrago MM, Schulz JB, Dichgans J, Luft AR (2004) Short and long-term motor skill learning in an accelerated rotarod training paradigm. Neurobiol Learn Mem 81:211–216.
Caggiano V, Leiras R, Goñi-Erro H, Masini D, Bellardita C, Bouvier J, Caldeira V, Fisone G, Kiehn O (2018) Midbrain circuits that set locomotor speed and gait selection. Nature 553:455–460.
Campos FL, Carvalho MM, Cristovão AC, Je G, Baltazar G, Salgado AJ, Kim Y-S, Sousa N (2013) Rodent models of Parkinson's disease: beyond the motor symptomatology. Front Behav Neurosci 7:175.
Cao V, Ye Y, Mastwal S, Ren M, Coon M, Liu Q, Costa R, Wang K (2015) Motor learning consolidates arc-expressing neuronal ensembles in secondary motor cortex. Neuron 86:1385–1392.
Capelli P, Pivetta C, Soledad Esposito M, Arber S (2017) Locomotor speed control circuits in the caudal brainstem. Nature 551:373–377.
Carvalho MM, Campos FL, Coimbra B, Pêgo JM, Rodrigues C, Lima R, Rodrigues AJ, Sousa N, Salgado AJ (2013) Behavioral characterization of the 6-hydroxidopamine model of Parkinson's disease and pharmacological rescuing of non-motor deficits. Mol Neurodegener 8:14.
Costa RM, Cohen D, Nicolelis MAL (2004) Differential corticostriatal plasticity during fast and slow motor skill learning in mice. Curr Biol 14:1124–1134.
Crawley JN (1999) Behavioral phenotyping of transgenic and knockout mice: experimental design and evaluation of general

health, sensory functions, motor abilities, and specific behavioral tests. Brain Res 835:18–26.
Darmohray DM, Jacobs JR, Marques HG, Carey MR (2019) Spatial and temporal locomotor learning in mouse cerebellum. Neuron 102:217–231.e4.
Durieux PF, Schiffmann SN, de Kerchove d'Exaerde A (2012) Differential regulation of motor control and response to dopaminergic drugs by D1R and D2R neurons in distinct dorsal striatum subregions. EMBO J 31:640–653.
Fitts PM (1954) The information capacity of the human motor system in controlling the amplitude of movement. J Exp Psychol 47:381–391.
Frigon A (2017) The neural control of interlimb coordination during mammalian locomotion. J Neurophysiol 117:2224–2241.
Haith AM, Krakauer JW (2013) Model-based and model-free mechanisms of human motor learning. Adv Exp Med Biol 782:1–21.
Harris CM, Wolpert DM (1998) Signal-dependent noise determines motor planning. Nature 394:780–784.
Hildebrand M (1965) Symmetrical gaits of horses. Science 150:701–708.
Joiner WM, Smith MA (2008) Long-term retention explained by a model of short-term learning in the adaptive control of reaching. J Neurophysiol 100:2948–2955.
Jones BJ, Roberts DJ (1968) The quantitative measurement of motor inco-ordination in naive mice using an accelerating rotarod. J Pharm Pharmacol 20:302–304.
Josset N, Roussel M, Lemieux M, Lafrance-Zoubga D, Rastqar A, Bretzner F (2018) Distinct contributions of mesencephalic locomotor region nuclei to locomotor control in the freely behaving mouse. Curr Biol 28:884–901.e3.
Krakauer JW, Ghazanfar AA, Gomez-Marin A, MacIver MA, Poeppel D (2017) Neuroscience needs behavior: correcting a reductionist bias. Neuron 93:480–490.
Kravitz AV, Freeze BS, Parker PRL, Kay K, Thwin MT, Deisseroth K, Kreitzer AC (2010) Regulation of parkinsonian motor behaviours by optogenetic control of basal ganglia circuitry. Nature 466:622–626.
Lemieux M, Josset N, Roussel M, Couraud S, Bretzner F (2016) Speed-dependent modulation of the locomotor behavior in adult mice reveals attractor and transitional gaits. Front Neurosci 10:42.
Li H-Q, Spitzer NC (2020) Exercise enhances motor skill learning by neurotransmitter switching in the adult midbrain. Nat Commun 11:2195.
Machado, A.S., Darmohray, D.M., Fayad, J., Marques, H.G., and Carey, M.R. (2015). A quantitative framework for whole-body coordination reveals specific deficits in freely walking ataxic mice. Elife 4.
Mandelblat-Cerf Y, Novick I, Vaadia E, Chapouthier G (2011a) Expressions of multiple neuronal dynamics during sensorimotor learning in the motor cortex of behaving monkeys. PLoS ONE 6: e21626.
Mandelblat-Cerf Y, Novick I, Paz R, Link Y, Freeman S, Vaadia E (2011b) The neuronal basis of long-term sensorimotor learning. J Neurosci 31:300–313.
Mathis A, Mamidanna P, Cury KM, Abe T, Murthy VN, Mathis MW, Bethge M (2018) DeepLabCut: markerless pose estimation of user-defined body parts with deep learning. Nat Neurosci 21:1281–1289.
Monville C, Torres EM, Dunnett SB (2006) Comparison of incremental and accelerating protocols of the rotarod test for the assessment of motor deficits in the 6-OHDA model. J Neurosci Methods 158:219–223.
Murray AJ, Croce K, Belton T, Akay T, Jessell TM (2018) Balance control mediated by vestibular circuits directing limb extension or antagonist muscle co-activation. Cell Rep 22:1325–1338.
Reisman DS, Wityk R, Silver K, Bastian AJ (2007) Locomotor adaptation on a split-belt treadmill can improve walking symmetry post-stroke. Brain 130:1861–1872.
Roseberry T, Lee AM, Lalive A, Wilbrecht L, Bonci A, Kreitzer A (2016) Cell-type-specific control of brainstem locomotor circuits by basal ganglia. Cell 164:526–537.
Sales-Carbonell C, Taouali W, Khalki L, Pasquet MO, Petit LF, Moreau T, Rueda-Orozco PE, Robbe D (2018) No discrete start/stop signals in the dorsal striatum of mice performing a learned action. Curr Biol 28:3044–3055.e5.
Sausbier M, Hu H, Arntz C, Feil S, Kamm S, Adelsberger H, Sausbier U, Sailer CA, Feil R, Hofmann F, et al. (2004) Cerebellar ataxia and Purkinje cell dysfunction caused by Ca2+-activated K+ channel deficiency. Proc Natl Acad Sci U S A 101:9474–9478.
Shadmehr R, Smith MA, Krakauer JW (2010) Error correction, sensory prediction, and adaptation in motor control. Annu Rev Neurosci 33:89–108.
Shiotsuki H, Yoshimi K, Shimo Y, Funayama M, Takamatsu Y, Ikeda K, Takahashi R, Kitazawa S, Hattori N (2010) A rotarod test for evaluation of motor skill learning. J Neurosci Methods 189:180–185.
Smith MA, Ghazizadeh A, Shadmehr R, Ashe J (2006) Interacting adaptive processes with different timescales underlie short-term motor learning. PLoS Biol 4:e179.
Sternad D (2018) It's not (only) the mean that matters: variability, noise and exploration in skill learning. Curr Opin Behav Sci 20:183–195.
Torres-Oviedo G, Vasudevan E, Malone L, Bastian AJ (2011) Locomotor adaptation. Prog Brain Res 191:65–74.
Wu HG, Miyamoto YR, Castro LNG, Ölveczky BP, Smith MA (2014) Temporal structure of motor variability is dynamically regulated and predicts motor learning ability. Nat Neurosci 17:312–321.
Xu-Wilson M, Chen-Harris H, Zee DS, Shadmehr R (2009) Cerebellar contributions to adaptive control of saccades in humans. J Neurosci 29:12930–12939.
Yin HH, Mulcare SP, Hilário MRF, Clouse E, Holloway T, Davis MI, Hansson AC, Lovinger DM, Costa RM (2009) Dynamic reorganization of striatal circuits during the acquisition and consolidation of a skill. Nat Neurosci 12:333–341.
Yttri EA, Dudman JT (2016) Opponent and bidirectional control of movement velocity in the basal ganglia. Nature 533:402–406.
Zhou X, Tien RN, Ravikumar S, Chase SM (2019) Distinct types of neural reorganization during long-term learning. J Neurophysiol 121:1329–1341.

## APPENDIX A. SUPPLEMENTARY DATA

Supplementary data to this article can be found online at https://doi.org/10.1016/j.neuroscience.2021.05.002.

*(Received 7 January 2021, Accepted 4 May 2021)*
*(Available online 24 May 2021)*